(Received 3 February 2024, Accepted 5 April 2024, Scheduled 11 April 2024)

A Novel Multi-Objective Synchronous Optimal Subarray Partition Method for Transmitting Array in Microwave Wireless Power Transmission

Jianxiong Li[1, 2, *] and Chen Wang[1, 2]

[1] School of Electronic and Information Engineering, Tiangong University, Tianjin, China
[2] Tianjin Key Laboratory of Optoelectronic Detection Technology and Systems, Tianjin, China

ABSTRACT: To improve the beam collection efficiency (*BCE*) of the microwave wireless power transmission (MWPT) system while reducing the peak sidelobe level outside the receiving area (*CSL*) and system cost, this paper proposes a new subarray partition technique and a nonuniform sparsely distributed quadrant symmetric planar array (NSDQSPA) model. A particle swarm optimization algorithm based on multiple-objective with nonlinear time-variant inertia and learning factor improved particle swarm optimization (MO-NTVILF-IPSO) is also proposed. The one-step multi-objective subarray partition algorithm adopts dynamic weight and dynamic learning factor to carry out one-step optimization on the array element arrangement of the transmitting array. The optimization algorithm simultaneously optimizes two performance indicators: the ΔBCE, which represents the optimization accuracy for the *BCE*, and the α_{ref}, which represents the mean square error of the excitation amplitude before and after the subarray partition. Many simulation results show that the *BCE* is 94.91%, and the *CSL* is -13.41 dB when the transmitting array with an aperture of $4.5\lambda \times 4.5\lambda$ is divided into six subarrays. The simulation results further demonstrate that the proposed subarray division method is appropriate for the MWPT system and that the algorithm in this paper, when the array elements with the same excitation amplitude are divided for the planar transmitting array on the array model, and can guarantee relatively high *BCE* and relatively low complexity of the system feed network.

1. INTRODUCTION

Microwave wireless power transmission (MWPT) technology was initially demonstrated in Nikola Tesla's coil experiment and has undergone continuous development for over a century. Compared with traditional power transmission technology, wireless power transmission is characterized by not transmitting power through wired cables, reducing system cost [1]. Recently, this technology has found extensive use in various domains, including wireless charging in remote mountainous regions, medical implants within the body, drones, Internet of Things devices, and space solar power stations (SPSS) [2–6]. Beam Collection Efficiency (*BCE*) is a critical parameter for evaluating the performance of the transmitting array of the MWPT system, which is defined as the proportion of the power collected by the receiving array to the total power radiated by the transmitting array. The peak sidelobe level outside the receiving area (*CSL*) is another critical parameter, representing the utilization of the radiation surface of the receiving array, and the lower the *CSL* is, the lower the power loss and the impact on the performance of other system components are [7]. Traditional transmitting arrays are often designed to transmit a strong microwave beam into a specific receiving area to achieve high *BCE* and minimize the *CSL*. The array elements are arranged according to the excitation amplitude, which is the curve of Gaussian distribution, with a higher excitation amplitude in the middle of the transmitting array and a lower excitation amplitude around [8]. Although this arrangement can achieve high *BCE*, the entire system requires many feed network amplifiers with different powers to provide different excitation amplitudes. In practical engineering, this array manufacturing is expensive and difficult to implement. Therefore, it is urgent to design an optimization model to achieve high *BCE* in the transmitting array and simplify the feed network complexity in the overall system.

To guarantee the power transmission needs of the MWPT system, it is essential to carefully evaluate both the transmitting performance of the array and the feed cost. Previous studies have optimized the position and excitation amplitude of the array elements and restricted the element spacing to prevent the occurrence of gate lobes and gate zeros. An optimization algorithm for uniformly excited nonuniform distributed planar arrays simplifies the feeder network and further decreases manufacturing cost [9]. However, this model will cause higher *CSL* and result in a loss of power transmission performance of the transmitting array, and the result of *BCE* is 91.06%. The optimization algorithm for nonuniform excitation nonuniform distributed planar arrays can achieve good power transmission performance, and the result of *BCE* is 96.45%. Because the excitation amplitude is different, many feed network amplifiers are required, which increases the cost. Recent research has adopted subarray partition technology. The array is grouped according to the excitation amplitude [10, 11], and the complete one-dimensional linear or two-dimensional planar array is divided into several groups. After dividing the subarrays, the entire ar-

* Corresponding author: Jianxiong Li (lijianxiong@tiangong.edu.cn).

ray element feed network and array structure are simplified, reducing the cost and the algorithm complexity during the data simulation [12]. The previous optimization method consists of two steps: the first is the arrangement position of the subarrays, followed by the excitation amplitude of the elements in the subarray [13–15]. This model has 64 array elements with an aperture of $4.5\lambda \times 4.5\lambda$. The optimization method performs better with more subarrays (number of subarrays greater than 8) but worse with fewer subarrays (number of subarrays less than 4).

Based on the previous research, this paper proposes a one-step multi-objective subarray partition algorithm based on nonlinear time variant-inertia and learning factor particle swarm optimization algorithm with nonuniform quadrant symmetric distribution, which is a multi-objective nonlinear particle swarm subarray partition algorithm for optimizing sparse planar arrays. This paper discusses the problem of subarray partition for sparsely distributed transmitting arrays. The main contributions are as follows: Firstly, unlike the multi-step optimization algorithm in [16], the algorithm used in this paper is a one-step optimization algorithm while optimizing the accuracy of *BCE* and the mean square error of excitation amplitude before and after partition. A large number of empirical evidences demonstrate that the outcomes of this optimization technique surpass those of alternative optimization techniques. Secondly, the proposed method improves the algorithm in [17], and the improved PSO algorithm suggested in this paper can achieve multi-objective synchronous optimization while learning multiple performance indicators. Meanwhile, in [18], Sun et al. proposed a multi-wave power conversion model that improved the *BCE*, but the result was only 92.82%, and a large number of array elements were required. In [19], Guo et al. used the invasive weed optimization (IWO) algorithm to optimize the array and made progress in reducing the *CSL*, but the enhancement of *BCE* was not obvious, and the result was only 92.60%. Finally, the superiority of the nonuniform sparsely distributed quadrant symmetric planar array (NSDQSPA) model over other array models was demonstrated. In this paper, the effectiveness of the algorithm is evaluated using the transmitting array performance parameters, including the *BCE*, *CSL*, ΔBCE and α_{ref}. In a MWPT system, the *BCE* is an indicator of the performance of the transmitting array, and the higher the *BCE* is, the better the performance of the transmitting array is. At the same time, for the improved PSO algorithm proposed in this paper, the optimization objective ΔBCE is the optimization accuracy of the *BCE* after each iteration. The ΔBCE, which can react to the optimization accuracy of the algorithm, and the higher the ΔBCE is, the better the performance of the algorithm is.

2. MATHEMATICAL DERIVATION OF EMISSION ARRAY AND SUBARRAY PARTITION

2.1. Mathematical Formula for Sparse Quadrant Symmetric Planar Array

Figure 1 displays the NSDQSPA model of the MWPT system. The transmitting array model suggested in this paper is based on a quadrant symmetric configuration, where the array elements

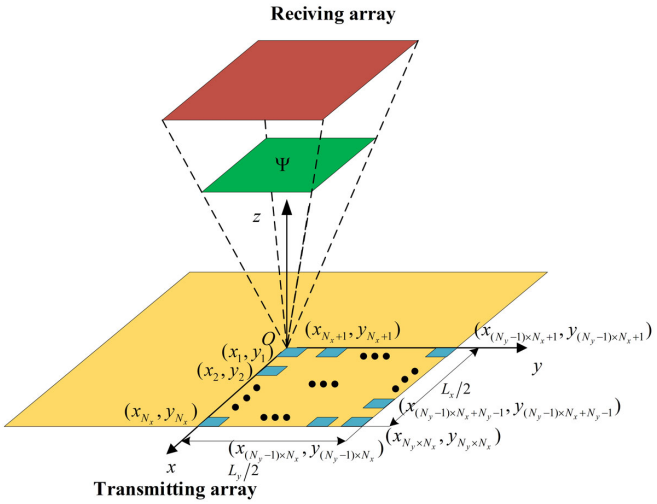

FIGURE 1. The NSDQSPA transmitting array model of the MWPT.

are spread symmetrically throughout the quadrants. The picture only displays the arrangement of the array elements in the first quadrant. The next three quadrants can be constructed by mapping the positions of the array elements in the first quadrant using symmetry.

The transmitting array concept suggested in this paper consists of $N = 4 \times N_x \times N_y$ array elements, with an aperture size of $L_x \times L_y$; the coordinate of the n-th array element is (x_n, y_n); and the corresponding excitation amplitude is α_n. As the transmitting model proposed in this paper is distributed symmetrically in quadrants, the research object is the first quadrant array element in the planar transmitting array. Therefore, the array factor formula for the transmitting array is:

$$F(u,v) = \sum_{n=1}^{N} \alpha_n e^{ik(ux_n + vy_n)} \tag{1}$$

where $k = 2\pi/\lambda$ is the wave number; λ is the wavelength; $u = \sin\theta\cos\varphi$ and $v = \sin\theta\sin\varphi$ are angular coordinates.

Define the receiving power area as:

$$\Psi = \{(u,v) : -u_0 \le u \le u_0,\ -v_0 \le v \le v_0\} \tag{2}$$

The entire visible area is:

$$\Omega = \{(u,v) : u^2 + v^2 \le 1\} \tag{3}$$

the *BCE* can be defined as the ratio of the radiation power of the receiving power area to the total power of the transmitting array, from Eq. (1), which can be written as:

$$BCE \triangleq \frac{P_\Psi}{P_\Omega} = \frac{\int\limits_\Psi |F(u,v)|^2 \, dudv}{\int\limits_\Omega |F(u,v)|^2 \, dudv} \tag{4}$$

where $F(u,v) = \mathbf{a}^H \mathbf{v}(u,v)$, according to [10], the *BCE* in Eq. (4) can also be expressed as:

$$BCE \triangleq \frac{P_\Psi}{P_\Omega} = \frac{\int_\Psi \mathbf{a}^H \mathbf{v}(u,v)\mathbf{v}^H(u,v)\mathbf{a} dudv}{\int_\Omega \mathbf{a}^H \mathbf{v}(u,v)\mathbf{v}^H(u,v)\mathbf{a} dudv} \tag{5}$$

where $\mathbf{a} = [\alpha_1, \alpha_2, ..., \alpha_N]^H$, $\mathbf{v}(u,v) = [e^{ik(ux_1+vy_1)}, ..., e^{ik(ux_N+vy_N)}]^H$, and the maximum *BCE* is written as:

$$BCE_{\max} = \frac{(\mathbf{a}_{\max})^H S_\Psi (\mathbf{a}_{\max})}{(\mathbf{a}_{\max})^H S_\Omega (\mathbf{a}_{\max})} \tag{6}$$

where S_Ψ represents the receiving area, S_Ω the entire visible area, and $\mathbf{a}_{\max}$ the optimal excitation amplitude for the transmitting array with subarray partition technology to obtain the maximum *BCE*. S_Ψ and S_Ω can be written as:

$$\begin{cases} S_\Psi \triangleq \int_\Psi \mathbf{v}(u,v)\mathbf{v}^H(u,v)dudv \\ S_\Omega \triangleq \int_\Omega \mathbf{v}(u,v)\mathbf{v}^H(u,v)dudv \end{cases} \tag{7}$$

In addition, the *CSL* represents the maximum utilization of the receiving area. It can also be used to evaluate the performance of the transmitting array, and a lower *CSL* indicates superior performance of the transmitting array. The *CSL* is defined as follows:

$$CSL\,(\text{dB}) = 10\lg \frac{\max_{\theta,\varphi\notin\Psi} |F(\theta,\varphi)|^2}{\max_{\theta,\varphi\in\Omega} |F(\theta,\varphi)|^2} \tag{8}$$

2.2. Mathematical Formula for Subarray Partition Model of Transmitting Array

This paper adopts array elements with nonuniform excitation amplitude with different excitation amplitudes for each subarray after dividing subarray. Assuming that the $N = 4 \times N_x \times N_y$ elements in the arrays are divided into M subarrays ($M < N$), C_{nm} is the weight matrix with a number of elements $N \times M$, where elements are 0 or 1.

$$C_{nm} = \begin{cases} 0 & \text{The } n\text{-th element } \notin \text{ the } m\text{-th subarray} \\ 1 & \text{The } n\text{-th element } \in \text{ the } m\text{-th subarray} \end{cases}$$
$$(m = 1, 2, ..., M;\ n = 1, 2, ..., N) \tag{9}$$

The weight matrix of the subarray partition can be expressed as:

$$\mathbf{C}_{nm} = \begin{bmatrix} C_{11} & C_{12} & ... & C_{1M} \\ C_{21} & C_{22} & \cdots & C_{2M} \\ \vdots & \vdots & \ddots & \vdots \\ C_{N1} & C_{N2} & \cdots & C_{NM} \end{bmatrix}_{N\times M} \tag{10}$$

This matrix represents a division from of subarray, where:

$$\sum_{m=1}^{M} C_{nm} = 1\,(n = 1, 2, ..., N) \tag{11}$$

This formula represents a subarray partition matrix where only one element in each row is 1, ensuring that each element is only divided into one subarray.

Assume that the excitation amplitude of each array element is:

$$\mathbf{a} = [\alpha_1, \alpha_2, ..., \alpha_N]^H \tag{12}$$

The excitation amplitude of each subarray after dividing the subarray is:

$$\mathbf{a}_{subm} = [\alpha_{sub1}, \alpha_{sub2}, ..., \alpha_{subM}]^H \tag{13}$$

where M subarrays have $M + 1$ boundaries, and these boundaries can be written as:

$$\mathbf{a}_{range} = \left[\alpha_{range_0}, \alpha_{range_1}, ..., \alpha_{range_M}\right]^H \tag{14}$$

The boundary processing condition is:

$$\alpha_{range_m} = \alpha_{\min} + m \times \frac{\alpha_{\max} - \alpha_{\min}}{M} \quad (m = 0, 1, ..., M) \tag{15}$$

where $\alpha_{\max}$ is the maximum initial excitation, and $\alpha_{\min}$ is the minimum initial excitation.

The excitation amplitude of the subarray can be calculated according to the following formula:

$$\alpha_{subm} = \frac{\sum_{n=1}^{N} \alpha_n \times C_{nm}}{\sum_{n=1}^{N} C_{nm}} \tag{16}$$

The total excitation amplitude can be expressed as:

$$\mathbf{a}_{sub} = \mathbf{C}_{nm} \times \mathbf{a}_{subm} \tag{17}$$

2.3. The Formula of Optimization Variable

The purpose of subarray partition is to maintain a relatively high *BCE*, while reducing the feed network complexity, thereby reducing manufacturing and maintenance cost. The optimization variable in this paper is the mean square error of the excitation amplitude of the elements before and after the subarray partition α_{ref}, and the other optimization variable is *BCE* optimization accuracy ΔBCE. Therefore, this paper optimizes these two indicators to improve the feasibility of the algorithm. One is α_{ref}, which can be written as:

$$\alpha_{ref} = \frac{1}{n} \sum_{i=1}^{N} (\alpha_{sub}(i) - \alpha(i))^2 \tag{18}$$

where $\alpha_{sub}(i)$ represents the excitation amplitude of individual element after dividing the subarray, and $\alpha(i)$ represents the excitation amplitude before dividing the subarray.

The other is ΔBCE, which can be written as:

$$\Delta BCE = BCE - BCE_{initial} \tag{19}$$

where the *BCE* can be calculated by Eq. (6), and $BCE_{initial}$ represents the initialized BCE without subarray partition under nonuniform excitation amplitude of uniformly distributed array elements.

3. MO-NTVILF-IPSO OPTIMIZATION ALGORITHM MODEL AND ITS APPLICATION IN NSDQSPA

3.1. The NSDQSPA Synthesis Model

From Figure 1, to ensure high *BCE* and low *CSL*, the NSQDSPA model is a quadrant symmetric model. The

calculation cost is reduced since the optimization process only needs to be performed once. Additionally, the remaining three quadrants can be symmetrically obtained, which reduces production and maintenance cost in engineering technology.

On the other hand, in order to prevent array coupling and gate lobe phenomenon caused by the small spacing of array elements, the constraint $d_{\min}$ between two random array elements during array placement is expressed as follows:

$$\sqrt{(x_i - x_j)^2 + (y_i - y_j)^2} \geq d_{\min}$$
$$i, j \in \{1, 2, ..., N\},\ i \neq j \tag{20}$$

Therefore, the horizontal and vertical coordinates of $N_x \times N_y$ array elements in the first quadrant are preprocessed while satisfying the minimum spacing $d_{\min}$ between the array elements, and the preprocessing matrix of the horizontal coordinates of the positions of each array element can be expressed as:

$$\begin{aligned}\mathbf{X} = &\begin{bmatrix} x_1 & x_2 & \cdots & x_{N_x} \\ x_{N_x+1} & x_{N_x+2} & \cdots & x_{2\times N_x} \\ \vdots & \vdots & \ddots & \vdots \\ x_{(N_y-1)\times N_x+1} & x_{(N_y-1)\times N_x+2} & \cdots & x_{N_y\times N_x} \end{bmatrix}_{N_y\times N_x} \\ = &\begin{bmatrix} dx_1 & dx_2 & \cdots & dx_{N_x} \\ dx_{N_x+1} & dx_{N_x+2} & \cdots & dx_{2\times N_x} \\ \vdots & \vdots & \ddots & \vdots \\ dx_{(N_y-1)\times N_x+1} & dx_{(N_y-1)\times N_x+2} & \cdots & dx_{N_y\times N_x} \end{bmatrix}_{N_y\times N_x} \\ + &\begin{bmatrix} 0 & d_{\min} & \cdots & (N_x-1)\times d_{\min} \\ 0 & d_{\min} & \cdots & (N_x-1)\times d_{\min} \\ \vdots & \vdots & \ddots & \vdots \\ 0 & d_{\min} & \cdots & (N_x-1)\times d_{\min} \end{bmatrix}_{N_y\times N_x} \\ = &\ \mathbf{D}_X + \mathbf{D}_{X_{\min}}\end{aligned} \tag{21}$$

The preprocessing matrix of the vertical coordinates of each array element position can be expressed as:

$$\begin{aligned}\mathbf{Y} = &\begin{bmatrix} y_1 & y_2 & \cdots & y_{N_x} \\ y_{N_x+1} & y_{N_x+2} & \cdots & y_{2\times N_x} \\ \vdots & \vdots & \ddots & \vdots \\ y_{(N_y-1)\times N_x+1} & y_{(N_y-1)\times N_x+2} & \cdots & y_{N_y\times N_x} \end{bmatrix}_{N_y\times N_x} \\ = &\begin{bmatrix} dy_1 & dx_2 & \cdots & dy_{N_x} \\ dy_{N_x+1} & dy_{N_x+2} & \cdots & dy_{2\times N_x} \\ \vdots & \vdots & \ddots & \vdots \\ dy_{(N_y-1)\times N_x+1} & dy_{(N_y-1)\times N_x+2} & \cdots & dy_{N_y\times N_x} \end{bmatrix}_{N_y\times N_x} \\ + &\begin{bmatrix} 0 & 0 & \cdots & 0 \\ d_{\min} & d_{\min} & \cdots & d_{\min} \\ \vdots & \vdots & \ddots & \vdots \\ (N_y-1)d_{\min} & (N_y-1)d_{\min} & \cdots & (N_y-1)\times d_{\min} \end{bmatrix}_{N_y\times N_x} \\ = &\ \mathbf{D}_Y + \mathbf{D}_{Y_{\min}}\end{aligned} \tag{22}$$

Perform preprocessing on the location coordinates of the array elements by simplifying the horizontal and vertical coordinate matrices $\mathbf{X}$ and $\mathbf{Y}$ of the optimized array elements to the sum of $\mathbf{D}_X$, $\mathbf{D}_{X_{\min}}$ and $\mathbf{D}_Y$, $\mathbf{D}_{Y_{\min}}$. These methods reduce the search space from $\mathbf{X}$ and $\mathbf{Y}$ to $\mathbf{D}_X$ and $\mathbf{D}_Y$, only optimizing $\mathbf{D}_X$ and $\mathbf{D}_Y$, reducing the amount of data processing, and accelerating the convergence speed of the optimization process.

Therefore, according to Eq. (20), Eq. (21), and Eq. (22), the process of a one-step optimization algorithm can be described as:

$$\begin{cases} \text{find } \mathbf{D}_X,\ \mathbf{D}_Y,\ \mathbf{a}_{subm} \\ \text{maximize } \Delta BCE = \max(\mathbf{D}_X,\ \mathbf{D}_Y) \\ \text{minimize } \alpha_{ref} = \min(\mathbf{a}_{subm}) \\ \text{subject to} \\ \quad \text{(a) } \sqrt{(x_i - x_j)^2 + (y_i - y_j)^2} \geq d_{\min} \\ \quad \text{(b) } d_{\min}/2 \leq x_n \leq L_x/2 \\ \quad \text{(c) } d_{\min}/2 \leq y_n \leq L_y/2 \\ \quad \text{(d) } (x_n, y_n) = \left(-x_{n-N/4}, y_{n-N/4}\right),\ n = \left\{\frac{N}{4}+1, ..., \frac{N}{2}\right\} \\ \quad \text{(e) } (x_n, y_n) = \left(-x_{n-N/2}, -y_{n-N/2}\right),\ n = \left\{\frac{N}{2}+1, ..., \frac{3N}{4}\right\} \\ \quad \text{(f) } (x_n, y_n) = \left(x_{n-3N/4}, -y_{n-3N/4}\right),\ n = \left\{\frac{3N}{4}+1, ..., N\right\} \\ \quad \text{(g) } \left(x_{N_x\times N_y},\ y_{N_x\times N_y}\right) = (L_x/2, L_y/2) \\ \quad \text{(h) } \alpha_1 \leq \alpha_{sub1} < \alpha_{sub2} < ... < \alpha_{subM} \leq \alpha_N \\ \qquad (i, j \in \{1, 2, ..., N\},\ i \neq j) \end{cases} \tag{23}$$

The algorithm optimizes the variables $\mathbf{D}_X$, $\mathbf{D}_Y$ and $\mathbf{a}_{subm}$, and the optimization objectives are to maximize the ΔBCE and minimize the α_{ref}.

Limitation (a) guarantees the minimum distance between the elements in the array. Limitations (b) and (c) define the scope of the particle search. Limitations (d), (e), and (f) represent the coordinates of the array elements in other quadrants, obtained through symmetric mapping in the first quadrant. Limitation (g) specifies the coordinates of the boundary array elements, which determine the array aperture. Lastly, limitation (h) can be utilized to determine the excitation amplitude of each subarray.

3.2. Description of the MO-NTVILF-IPSO Optimization Algorithm

The MO-NTVILF-IPSO optimization algorithm is a one-step multi-objective optimization algorithm applied in the process of subarray partition for the transmitting array, and it can achieve good array performance with the same array aperture size and fewer array elements [20].

The optimization algorithm steps are as follows:

Step 1: Define parameters related to the transmitting array, including initial element position (x_n, y_n); minimum element spacing is $d_{\min}$; number of elements is $N = 4 \times N_x \times N_y$; array aperture is $L_x \times L_y$; number of subarrays is M; and receiving area is Ψ.

Step 2: Set the parameters in the optimization algorithm: the number of particles *NP*, the number of algorithm iterations *Epoch*, time-variant inertia weight upper limit $w_{\max}$ and lower

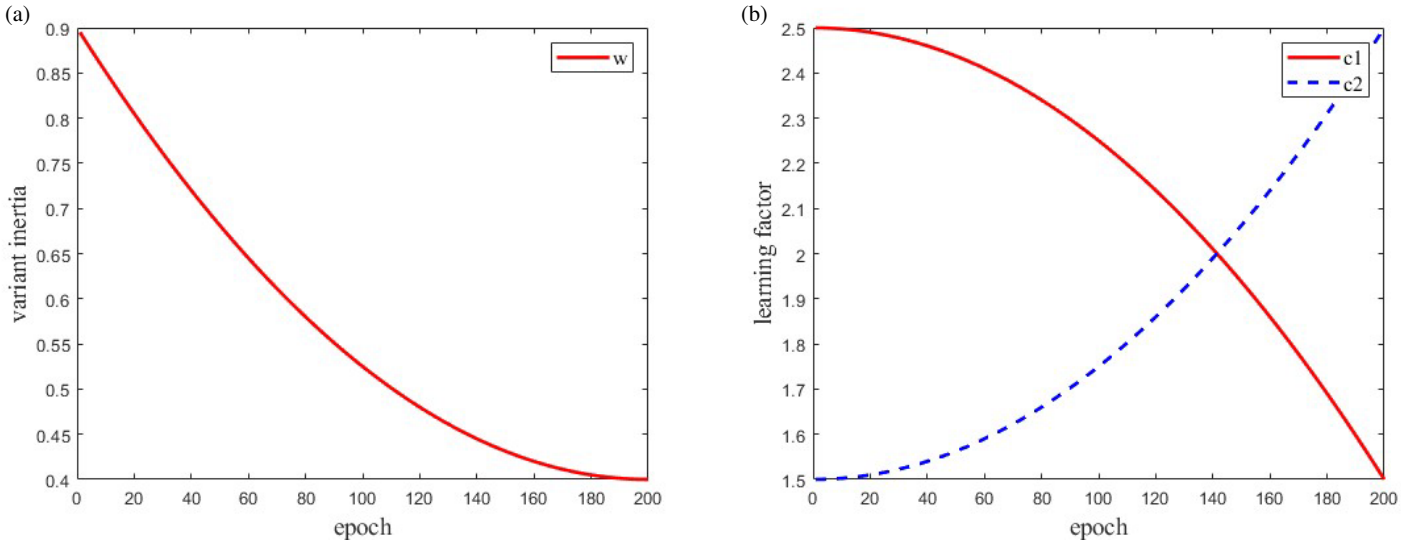

FIGURE 2. The parameters in MO-NTVILF-IPSO. (a) Time variant inertia. (b) Dynamic learning factor.

limit $w_{\min}$, dynamic learning factor upper limit $c_{\max}$ and lower limit $c_{\min}$, and particle position update speed v.

Step 3: Calculate the relevant parameters, including $BCE_{initial}$, $\mathbf{a}_{subm}$, and BCE.

Step 4: Calculate optimization parameters from Eq. (18) and Eq. (19); iterative updates are used to calculate the ΔBCE and w_{ref}; then select the personal optimal fitness values $pbest(1)$ and $pbest(2)$, global optimal fitness values $gbest(1)$ and $gbest(2)$.

Step 5: Utilizing the update formula inside the MO-NTVILF-IPSO algorithm, proceed to modify and save the velocity and location of the optimized particles. The updated formula is as follows:

$$\begin{aligned} v_t &= w \times v_{t-1} + c_1 \times rand\,(pbest(1)x_{t-1} - x_{t-1} \\ &\quad + pbest(2)x_{t-1} - x_{t-1}) + c_2 \times rand\,(gbest(1)x_{t-1} \\ &\quad - x_{t-1} + gbest(2)x_{t-1} - x_{t-1}) \end{aligned} \tag{24}$$

$$x_t = x_{t-1} + v_t \tag{25}$$

Step 6: As the number of iterations increases, the variant inertia weight w, learning factors c_1 and c_2, and local optimal fitness values of the particles in the next generation are updated.

Step 7: Check whether the maximum number of iterations has been achieved. If it has, display the highest global optimum fitness value $gbest(1)$ and the lowest global ideal fitness value $gbest(2)$. If the condition is not met, go back to Step 5 in order to resume the execution process.

3.3. Nonlinear Time Variant Inertia and Learning Factor

In the optimization technique presented in this work, *epoch* refers to the current iteration number, while *Epoch* represents the maximum iteration number.

The formula for updating time variant inertia weight is:

$$w = w_{\min} + (w_{\max} - w_{\min}) \times \left(\frac{Epoch - epoch}{Epoch}\right)^2 \tag{26}$$

The formula for updating the learning factor is:

$$\begin{aligned} c_1 &= c_{\min} + (c_{\max} - c_{\min}) \times \left[1 - \left(\frac{epoch}{Epoch}\right)^2\right] \\ c_2 &= c_{\max} + (c_{\min} - c_{\max}) \times \left[1 - \left(\frac{epoch}{Epoch}\right)^2\right] \end{aligned} \tag{27}$$

As shown in Figure 2, as the number of iterations grows, the weight w in PSO is nonlinear and time-varying, where $w_{\max}$ is the highest inertia weight, and $w_{\min}$ is the lowest inertia weight. The learning factors in PSO are also nonlinear and time-varying, with the maximum learning factor $c_{\max}$ and the minimum learning factor $c_{\min}$. For the inertia weight w, the range of particle optimization can be determined, since particles are required to search within the entire search range at the beginning, and the inertia weight is relatively large. The inertia weight can gradually decrease as the iteration progresses, achieving a good convergence effect. Therefore, this paper adopts nonlinear decreasing inertia weight. For the learning factors c_1 and c_2, they can determine the method of particle optimization. When $c_1 > c_2$, there is faster global search ability but slower convergence, when $c_1 < c_2$, it is more conducive to local search. Therefore, dynamic adjustment can make c_1 in the iteration process continuously decrease and c_2 increase, ensuring the initial stages particle search capability while preventing convergence to local optima in the subsequent phase, which is beneficial for improving the optimization results. The inertia weights used in this paper are: $w_{\max} = 0.9$, $w_{\min} = 0.4$, and the learning factor: $c_{\max} = 2.5$, $c_{\min} = 1.5$.

4. RESULTS AND DISCUSSION OF NUMERICAL SIMULATIONS

This section discusses and validates the superiority of the proposed NADQSPA model and MO-NTVILF-IPSO algorithm.

TABLE 1. Comparison of results of different array synthesis models.

Parameter	NSQDSPA	Method in [16]	Method in [10]	Method in [12]	Method in [18]	Method in [19]
N	64	100	100	64	316	79
M	6	1	100	6	4	10
BCE	94.92%	91.06%	96.45%	91.09%	92.82%	92.60%
CSL (dB)	−13.41	−16.01	−12.27	−14.48	−20.62	−11.97
γ_e	64%	100%	100%	64%	79%	79%
γ_a	12.5%	1%	100%	12.5%	1.2%	12.66%

Numerical simulation and result analysis are divided into five parts. The first part compares the proposed synthesis model with the other three planar array subarray partition models using some performance parameters. In the second part, the proposed algorithm and performance indicators are used to optimize the composite model under different numbers of subarrays, and the optimization results are obtained and compared. The third part compares the positions of the elements before and after the optimization algorithm and the excitation amplitude intensity of the subarrays. The fourth part validates the rationality of the proposed element spacing in this article. The final part compares the performance of the MO-NTVILF-IPSO algorithm with other PSO algorithms. The device used in this simulation is a PC processor with Intel Core i5-8300H 2.30 GHz, RAM of 16 GB, and the simulation and analysis software is MATLAB R2022b.

This paper uses ΔBCE, α_{ref}, *BCE*, and *CSL* as the performance indicators, and two sparse parameters are introduced as the evaluation indicators of the system cost since the studied array model is a sparse array. The sparsity of the array excitation amplitude amplifier $\gamma_a \triangleq \frac{M}{N}$ expresses the proportion of the number of array amplifiers to the number of arrays, and the sparsity of the number of array elements $\gamma_e \triangleq \frac{N}{N_{full}}$ represents the proportion of the number of sparsely distributed array elements to the number of full array elements with the same aperture. The receiving area is a rectangular area Ψ, and the rectangular power receiving area is defined as: $\Psi \triangleq \{(u,v) : -u_0 \le u \le u_0, -v_0 \le v \le v_0\}$, where $u_0 = v_0 = 0.2$.

All the simulation experiments in this section use: the number $N = 4 \times N_x \times N_y = 64$ and the aperture $4.5\lambda \times 4.5\lambda$ of the transmitting array. Meanwhile, to minimize the number of data computations, before the simulation, the wavelength λ of the transmitting array is normalized. As the object of this paper is a sparse array, the number of transmitting array elements should be sparsely processed to meet the requirements $d_{\min} \ge 0.5\lambda$ of the spacing of the array elements. Therefore, the spacing of the array elements in this simulation is taken simultaneously to achieve better optimization results, and the iterations of the algorithm number is set to $Epoch = 200$ and the optimized particles number set to $NP = 50$.

4.1. Comparison of Performance and System Cost between the NSDQSPA Synthesis Model and Other Array Models

This part conducts a comparative analysis between the proposed NSDQSPA model and three alternative optimization models for transmitting array synthesis. The aim was to evaluate and validate the effectiveness of the NSDQSPA model in improving both the performances of the transmitting array and the overall system cost.

Table 1 demonstrates the configuration of a sparsely distributed transmitting array. The array has the same aperture and receiving area, and is divided into six subarrays. In contrast to the synthetic model presented in [16], which uses a homogeneous excitation amplitude, not only the synthesis model proposed in this paper has higher *BCE* ($BCE = 94.92\% > BCE = 91.06\%$), but also the sparsity parameter of the composite model is lower than the sparsity parameter of the reference model ($\gamma_e = 64\% < \gamma_e = 100\%$). Reducing sparsity in practical engineering design can decrease the quantity of incorrect components in array layout and result in a decrease in system cost. Compared with the nonuniform excitation amplitude synthetic model proposed in [10], although the *BCE* of this synthesis model is lower ($BCE = 94.92\% < BCE = 96.45\%$), it has significant advantages in the sparsity parameters of the array element excitation amplifier and the number of array elements ($\gamma_e = 64\% < \gamma_e = 100\%, \gamma_a = 12.5\% < \gamma_a = 100\%$). The NSDQSPA model offers the advantage of minimizing the quantity of feed network amplifiers and array elements in the transmitting array, resulting in cost reduction in actual engineering applications. Additionally, it achieves a harmonious equilibrium between efficiency and cost. In contrast to the model presented in [12], the synthetic model described in this paper greatly enhances *BCE* of the sparse transmitting array using the subarray partition model ($BCE = 94.92\% > BCE = 91.09\%$). Unlike the model proposed in [18], the model proposed in this paper uses a small number of array elements, achieving higher *BCE* ($BCE = 94.92\% > BCE = 92.82\%$) and lower *CSL* ($CSL = -20.62\,\text{dB} < CSL = -13.41\,\text{dB}$). At the same time, the reduction in the number of arrays reduces the cost of the system. Compared to [19], the model proposed in this paper has a better transmitting performance ($BCE = 94.92\% > BCE = 92.60\%$) and also has an advantage in the sparsity of the array ($\gamma_e = 64\% < \gamma_e = 79\%$).

M	BCE	CSL (dB)	α_{ref}	ΔBCE
2	89.06%	−12.03	0.0156	−0.0537
3	93.09%	−11.03	0.0103	−0.0134
4	94.21%	−11.84	0.0020	−0.0022
5	94.59%	−13.29	3.30×10^{-4}	0.0016
6	94.92%	−13.40	2.38×10^{-6}	0.0049
7	95.13%	−12.65	1.41×10^{-31}	0.0070
8	95.16%	−12.76	7.73×10^{-34}	0.0073
9	95.17%	−13.14	0.0000	0.0074
10	95.27%	−12.68	0.0000	0.0084

TABLE 2. The MO-NTVILF-IPSO partition results with different numbers of subarrays on NSDQSPA model.

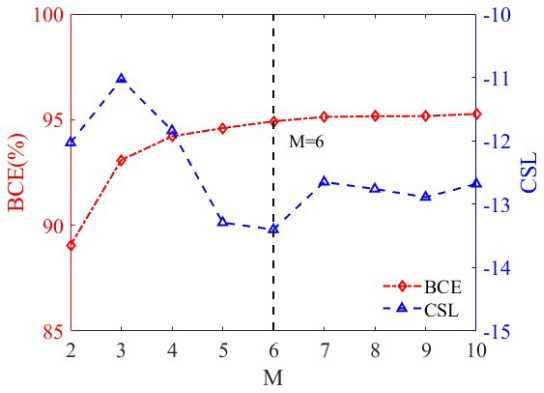

FIGURE 3. The *BCE* and *CSL* results of the MO-NTVILF-IPSO algorithm optimization model.

TABLE 3. The maximum excitation amplitude with different numbers of subarrays.

M	**2**	**3**	**4**	**5**	**6**	**7**	**8**	**9**	**10**
$\alpha_{\max}$	0.83	0.87	0.90	0.91	0.92	0.93	0.96	1.00	1.00

To summarize, compared to other synthetic models with sparse transmitting arrays, the NSDQSPA model greatly enhances the *BCE* of the transmitting arrays. Furthermore, the NSDQSPA model exhibits a reduced *BCE* compared to the full array, due to the quadrant symmetric arrangement of its parts. Nevertheless, the model decreases the expense of manufacturing and the intricacy of the feed network in real world engineering applications, ultimately resulting in a reduction in the overall system cost. Hence, this model is better suited for synthesizing transmitting arrays in the MWPT system.

4.2. Performance of MO-NTVILF-IPSO Algorithm in NSDQSPA Synthesis Model with Different Number of Subarrays

The simulation experiment in this section uses the MO-NTVILF-IPSO algorithm to optimize the NSDQSPA synthesis model with nonuniform excitation amplitude. The sparsity of the element excitation amplifier is $\gamma_a = 12.5\%$, whereas the sparsity of the number of array elements is $\gamma_e = 64\%$. The performance indicators suggested in this paper α_{ref} and ΔBCE are utilized for evaluation, and the results of the numerical simulation are displayed in Table 2.

As shown in Table 2, for the *BCE*, the excitation amplitude of the elements in the middle area of the transmitting array gradually increases. In contrast, the excitation amplitude of the elements in the surrounding area decreases. Therefore, the *BCE* increases when the number of subarrays is 6 ($M = 6$, $BCE = 94.92\%$), but the increase in *BCE* is not significant when $M > 6$. For the *CSL*, when the number of subarrays is 2, the *CSL* outside the receiving area is low ($M = 2$, $CSL = -12.03$ dB); when the number of subarrays exceeds 6, the *CSL* gradually decreases ($M = 7$, $CSL = -12.65$ dB), ($M = 8$, $CSL = -12.76$ dB), ($M = 9$, $CSL = -13.14$ dB), ($M = 10$, $CSL = -12.68$ dB). The optimization results of this algorithm on the *BCE* and *CSL* are shown in Figure 3. Therefore, it can be concluded that at $M = 6$, the overall performance of the array is good (*BCE* is higher, and *CSL* is lower), and this partition method is suitable for use in the MWPT system.

Meanwhile, as shown in Table 3, Figure 4, and Figure 5, after normalizing the maximum excitation amplitude of the subarray increases gradually with the number of partition subarrays ($M = 10$, $\alpha_{\max} = 1.00$) > ($M = 2$, $\alpha_{\max} = 0.83$), further proving that subarray partition of the transmitting array can improve array performance.

In order to further demonstrate the effectiveness of the composite model in dividing sparse transmitting arrays into subarrays, the evaluation indicators proposed in Eq. (18) and Eq. (19), namely α_{ref} and ΔBCE are used to evaluate the synthesis model. From Figure 6, it can be seen that as the number of subarray partitions increases, the optimization accuracy of the algorithm proposed in this paper for the *BCE* continuously improves. At the same time, the mean square error of the excitation amplitude before and after the subarray partition is reduced. The following conclusion can be reached that the algorithm is applicable in the subarray partition model of the transmitting array, and when the divided subarrays are greater than 5 ($M = 5:\ \Delta BCE = 0.0016$, $\alpha_{ref} = 3.30 \times 10^{-4}$), the optimization accuracy of the algorithm continues to improve. However, the improvement speed is slow; the mean square error is small; and good results can be achieved when dividing the number of subarrays into 6 ($M = 6:\ \Delta BCE = 0.0049$, $\alpha_{ref} = 2.38 \times 10^{-6}$). Therefore, dividing the transmitting array into six subarrays can effectively improve the performance of the transmitting array, and the model only uses six excitation amplitude amplifiers, reducing system cost.

Meanwhile, due to the nonuniform excitation amplitude of the arrays in the synthesis model, in order to verify the effec-

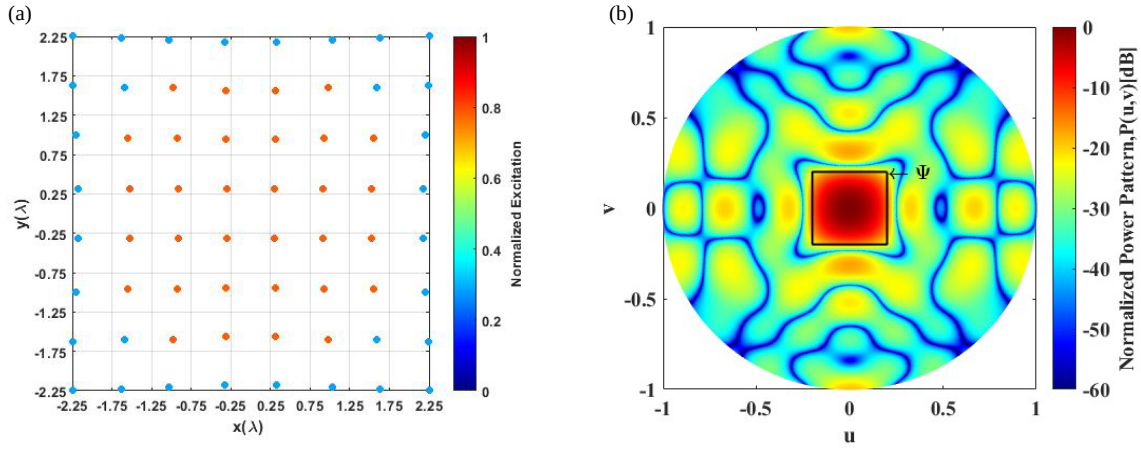

FIGURE 4. The simulation results of the NSDQSPA model with MO-NTVILF-IPSO algorithm, (a) excitation amplitude distribution, (b) normalized power pattern. ($M = 2$, $BCE = 89.06\%$, $CSL = -12.03\,\text{dB}$).

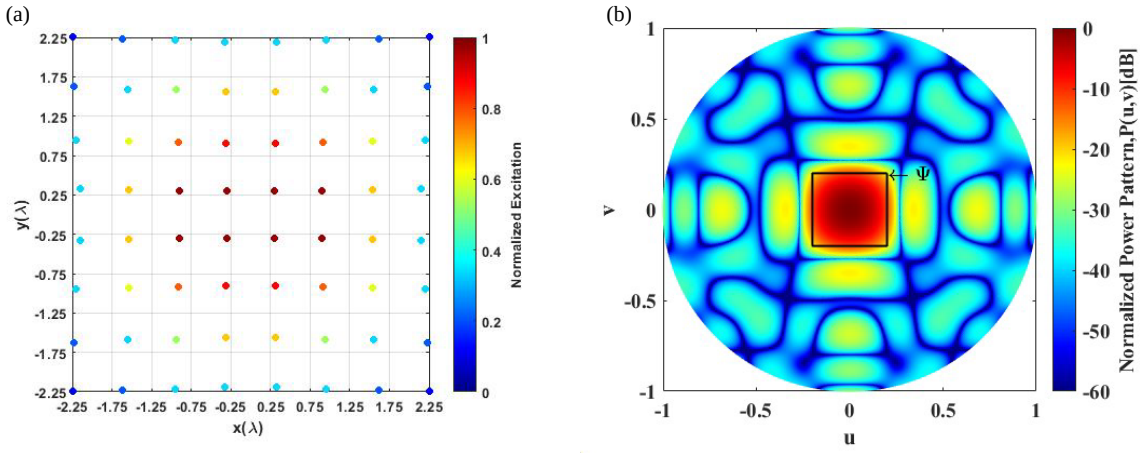

FIGURE 5. The simulation results of the NSDQSPA model with MO-NTVILF-IPSO algorithm, (a) excitation amplitude distribution, (b) normalized power pattern. ($M = 10$, $BCE = 95.27\%$, $CSL = -12.68\,\text{dB}$).

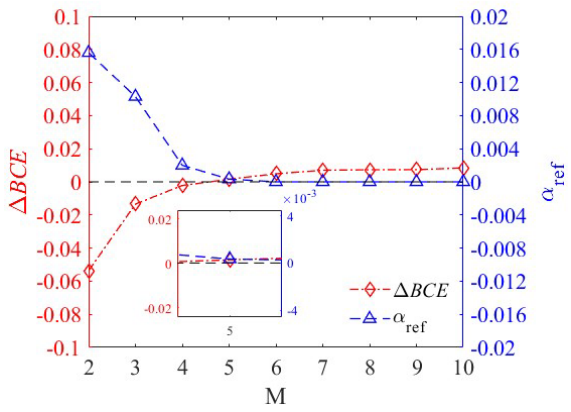

FIGURE 6. The ΔBCE and α_{ref} results of the MO-NTVILF-IPSO algorithm optimization model.

tiveness of the algorithm in optimizing the nonuniform excitation amplitude transmitting array with the same number of arrays, a comparison was made between the array excitation amplitude distribution and normalized power pattern not optimized by the algorithm, as shown in Figure 7. The array excitation amplitude distribution and normalized power pattern are optimized by the algorithm, as shown in Figure 8.

From the excitation amplitude distribution and normalized power pattern, it can be seen that when the number of subarrays is divided into 6, optimizing the subarray partition algorithm can concentrate the transmitting beams mainly in the central collection area, effectively reducing the impact of *CSL* out of the receiving area on the transmitting array ($CSL = -12.24\,\text{dB} < CSL = -11.21\,\text{dB}$). Moreover, the *BCE* is higher than that of the nonuniform excitation amplitude transmitting array optimized by the algorithm ($BCE = 94.92\% > BCE = 94.43\%$). The conclusion can be drawn that optimizing the quadrant symmetric model through this algorithm effectively improves the performance of the transmitting array.

4.3. Optimization of Element Position in MO-NTVILF-IPSO Algorithm

As shown in Figure 9, the algorithm can divide the array into subarrays according to the excitation amplitude while optimiz-

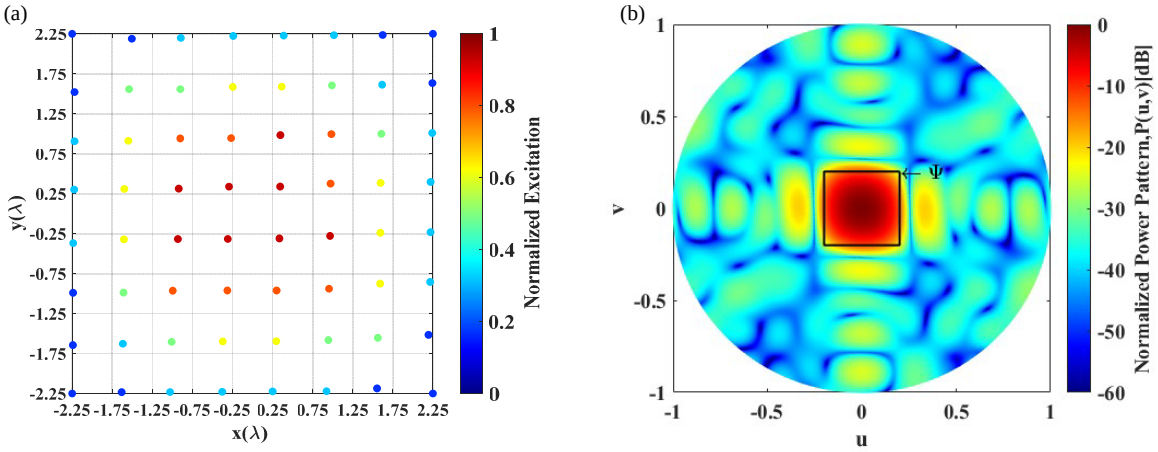

FIGURE 7. The simulation results of the NSDQSPA model without MO-NTVILF-IPSO algorithm, (a) excitation amplitude distribution, (b) normalized power pattern. ($M = 6$, $BCE = 94.43\%$, $CSL = -11.21$ dB).

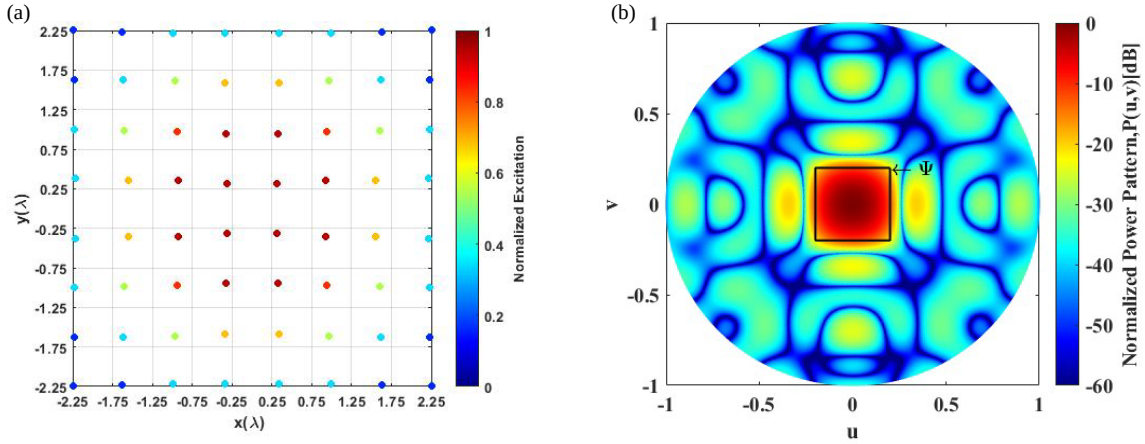

FIGURE 8. The simulation results of the NSDQSPA model without MO-NTVILF-IPSO algorithm, (a) excitation amplitude distribution, (b) normalized power pattern. ($M = 6$, $BCE = 94.92\%$, $CSL = -12.24$ dB).

ing the position of the array elements. With one-step multi-objective optimization, the performance of the optimized transmitting array is improved. Since the model is a quadrant symmetric model, the algorithm only optimizes the variables in the first quadrant when optimizing the model, and the rest of the quadrants can be mapped synchronously, which saves the expenditure of computational data of the system and improves the performance of the transmitter array model. Dividing the number of subarrays into 6 may significantly enhance the performance of the transmitting array using the technique ($BCE = 94.92\% > BCE = 76.10\%$), ($CSL = -13.40$ dB $< CSL = -12.30$ dB).

The excitation amplitudes of the subarrays have been normalized to values of 0.17, 0.31, 0.54, 0.63, 0.76, and 0.92. The distribution of these amplitudes may be seen in Figure 10.

4.4. Performance of the MO-NTVILF-IPSO Algorithm with Different Array Spacing

To further validate the superiority and rationality of the suggested spacing between array elements in this research, while also meeting the criteria for array sparsity [21], the performances of the array element spacing at 0.5λ, 0.55λ, and 0.6λ are compared using the evaluation metrics ΔBCE and α_{ref}.

From Figure 11, it can be seen that for different array element spacings, as the number of subarrays increases, ΔBCE increases, and α_{ref} decreases, which further proves that the subarray division method can improve the performance of the transmitting array. In the case of 6 subarrays, for the performance indicators of the array: the $\Delta BCE(0.6\lambda > 0.55\lambda > 0.5\lambda)$, $\alpha_{ref}(0.6\lambda < 0.55\lambda < 0.5\lambda)$, it can be concluded that for both ΔBCE and α_{ref}, the performance of the transmitting array is best for an array element spacing of 0.6λ, when the spacing of the array elements is chosen to be 0.65λ or 0.7λ, for the transmitting array with the same aperture, the number of array elements will be reduced, and at the same time the array performance will be reduced; therefore the array element spacing of 0.6λ is chosen.

4.5. Performance Comparison of MO-NTVILF-IPSO Algorithm with Other PSO Algorithms

To showcase the efficiency and superiority of the MO-NTVILF-IPSO algorithm suggested in this study, the algorithm

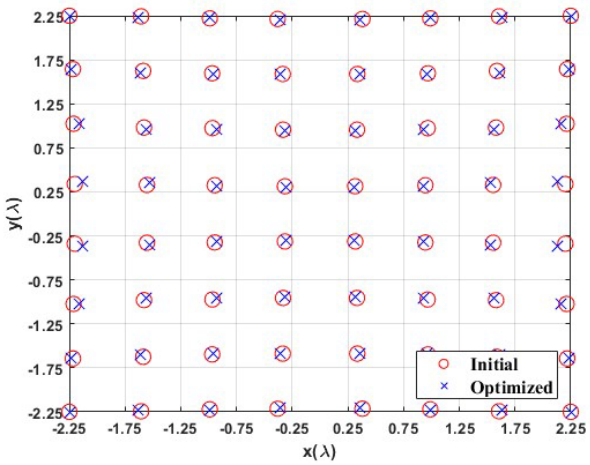

FIGURE 9. Distribution of transmitting array element positions before and after algorithm optimization.

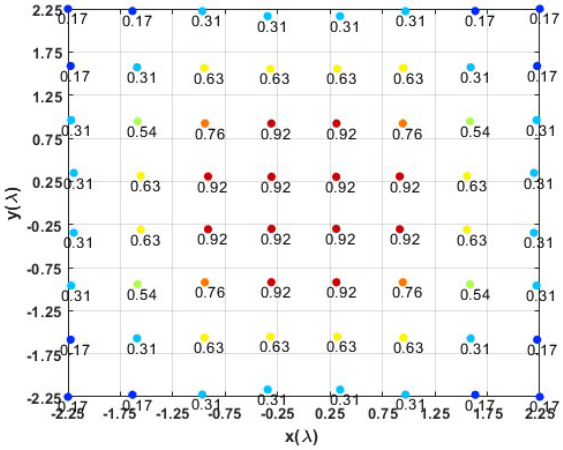

FIGURE 10. The excitation amplitude distribution of the optimization model.

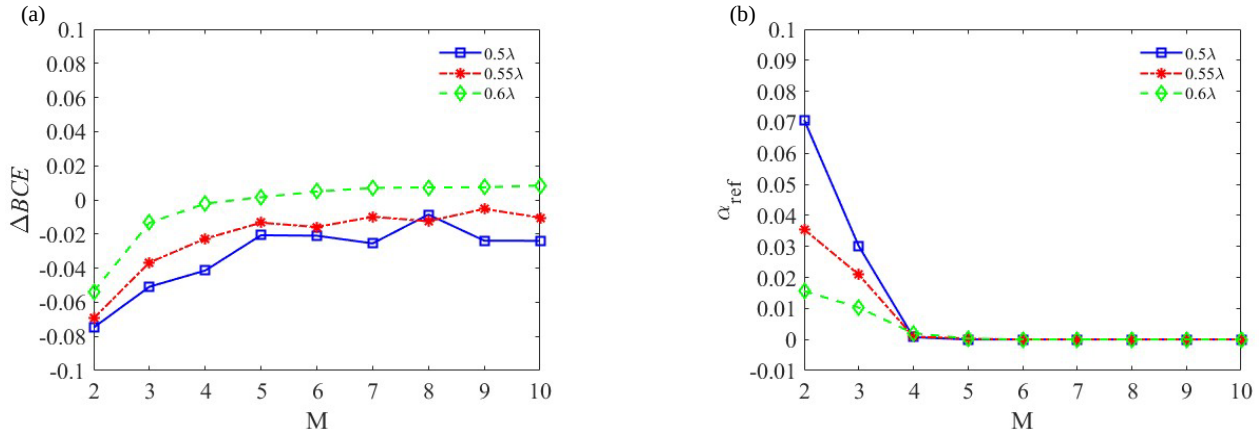

FIGURE 11. Performance comparison for different array spacing, (a) beam collection efficiency optimization accuracy ΔBCE, (b) excitation amplitude mean square error α_{ref}.

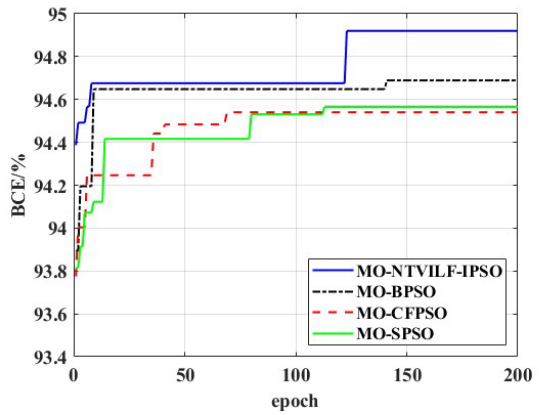

FIGURE 12. Comparison of *BCE* simulation results between MO-NTVILF-IPSO algorithm and other PSO algorithms.

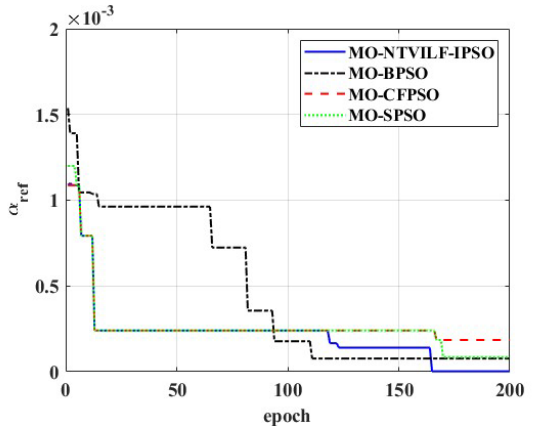

FIGURE 13. Comparison of α_{ref} simulation results between MO-NTVILF-IPSO algorithm and other PSO algorithms.

was implemented alongside three other PSO algorithms on the NSDQSPA model, using a transmitting array divided into six subarrays as the experimental setup.

As shown in Figures 12 and 13, the following conclusions can be drawn from the simulation experiment of 200 epochs of simulation experiments, the optimal *BCE* and α_{ref} obtained by

the proposed MO-NTVILF-IPSO algorithm is better than those of the multiple-objective basic particle swarm optimization algorithm (MO-BPSO) [22], multiple-objective standard particle swarm optimization algorithm (MO-SPSO) [23], and multiple-objective compression factor particle swarm optimization algorithm (MO-CFPSO) [24]. MO-CFPSO does not take into account the connection among global and local optima. Compared to the MO-BPSO algorithm, the results obtained by MO-NTVILF-IPSO algorithm can avoid local optima. Compared to MO-SPSO algorithm, which only changes the inertia weight linearly, MO-NTVILF-IPSO algorithm adopts dynamically adjusted learning factors and variable inertia weights to obtain better results. Compared to MO-CFPSO algorithm, MO-CFPSO algorithm has a slow convergence speed and is prone to fall into local optimality. Nevertheless, the proposed MO-NTVILF-IPSO algorithm conducts a global search at the initial stage of each iteration and a local search at a later stage. This approach enhances both the speed of convergence and the guarantee of achieving a convergence result.

5. CONCLUSION

In this paper, an NSDQSPA model is proposed to optimize the performance of a transmitting array. The model is divided into subarrays based on the excitation amplitude of each subarray, and MO-NTVILF-IPSO algorithm is proposed as a one-step optimization algorithm that simultaneously optimizes ΔBCE of the transmitting array and the α_{ref} before and after dividing the subarrays. According to the proposed array optimization model and algorithm, good results have been achieved in terms of improving the performance of the transmitting array and reducing system cost.

The effectiveness of the models and algorithms proposed in this paper can be tested by analyzing a large number of data simulations. By comparing the proposed array model with several known models, the superiority of the proposed model is confirmed through several performance evaluation indicators, such as the sparsity parameter, *BCE*, and *CSL*. The simulation results obtained in this article on the NSDQSPA transmitting model with the transmitting aperture of $4.5\lambda \times 4.5\lambda$ and the receiving area of $u_0 = v_0 = 0.2$ are as follows: The optimal element spacing is 0.6λ, and when the overall transmitting array is divided into 6 subarrays, the sparsity parameters of the model are: $\gamma_a = 12.5\%$, $\gamma_e = 64\%$; simultaneously the transmitting array performance parameters: $BCE = 94.92\%$, $CSL = -13.4$ dB. Compared to arrays with the same elements that are not under a subarray partition, the optimization accuracy is $\Delta BCE = 0.0049$ and $\alpha_{ref} = 2.38 \times 10^{-6}$. The optimization technique presented in this paper may significantly enhance the performance of the transmitting array in the MWPT system. The method enhances the *BCE* and reduces the reference error compared to arrays that have nonuniform excitation amplitude. Additionally, the model adopts quadrant symmetric distribution, which saves system cost and is suitable for the MWPT system.

ACKNOWLEDGEMENT

This work was supported by the National Natural Science Foundation of China (Grant No. 51877151) and the Program for Innovative Research Team in University of Tianjin (Grant No. TD13-5040).

REFERENCES

[1] Lu, F., H. Zhang, W. Li, Z. Zhou, C. Zhu, C. Cheng, Z. Deng, X. Chen, and C. C. Mi, "A high-efficiency and long-distance power-relay system with equal power distribution," *IEEE Journal of Emerging and Selected Topics in Power Electronics*, Vol. 8, No. 2, 1419–1427, 2020.

[2] Lee, C. H., G. Jung, K. A. Hosani, B. Song, D.-K. Seo, and D. H. Cho, "Wireless power transfer system for an autonomous electric vehicle," in *2020 IEEE Wireless Power Transfer Conference (WPTC)*, 467–470, 2020.

[3] Li, X., B. Duan, L. Song, Y. Yang, Y. Zhang, and D. Wang, "A new concept of space solar power satellite," *Acta Astronautica*, Vol. 136, 182–189, 2017.

[4] Li, X., J. Zhou, B. Duan, Y. Yang, Y. Zhang, and J. Fan, "Performance of planar arrays for microwave power transmission with position errors," *IEEE Antennas and Wireless Propagation Letters*, Vol. 14, 1794–1797, 2015.

[5] Li, Y. and V. Jandhyala, "Design of retrodirective antenna arrays for short-range wireless power transmission," *IEEE Transactions on Antennas and Propagation*, Vol. 60, No. 1, 206–211, 2012.

[6] Chen, Q., X. Chen, and P. Feng, "A comparative study of space transmission efficiency for the microwave wireless power transmission," in *2015 Asia-Pacific Microwave Conference (APMC)*, Vol. 3, 1–3, Nanjing, China, Dec. 2015.

[7] Massa, A., G. Oliveri, F. Viani, and P. Rocca, "Array designs for long-distance wireless power transmission: State-of-the-art and innovative solutions," *Proceedings of the IEEE*, Vol. 101, No. 6, 1464–1481, 2013.

[8] Li, X., B. Duan, L. Song, Y. Zhang, and W. Xu, "Study of stepped amplitude distribution taper for microwave power transmission for SSPS," *IEEE Transactions on Antennas and Propagation*, Vol. 65, No. 10, 5396–5405, 2017.

[9] Shi, Q., Z. Zheng, and Y. Sun, "Pattern synthesis of subarrayed large linear and planar arrays using K-means solution," *IEEE Antennas and Wireless Propagation Letters*, Vol. 20, No. 5, 693–697, 2021.

[10] Oliveri, G., L. Poli, and A. Massa, "Maximum efficiency beam synthesis of radiating planar arrays for wireless power transmission," *IEEE Transactions on Antennas and Propagation*, Vol. 61, No. 5, 2490–2499, 2013.

[11] Anselmi, N., A. Polo, M. A. Hannan, M. Salucci, and P. Rocca, "Maximum BCE synthesis of domino-tiled planar arrays for far-field wireless power transmission," *Journal of Electromagnetic Waves and Applications*, Vol. 34, No. 17, 2349–2370, 2020.

[12] Xiong, Z.-Y., Z.-H. Xu, S.-W. Chen, and S.-P. Xiao, "Subarray partition in array antenna based on the algorithm X," *IEEE Antennas and Wireless Propagation Letters*, Vol. 12, No. 12, 906–909, 2013.

[13] Li, J. and S. Chang, "Novel sparse planar array synthesis model for microwave power transmission systems with high efficiency and low cost," *Progress In Electromagnetics Research C*, Vol. 115, 245–259, 2021.

[14] Li, J., J. Pan, and X. Li, "A novel synthesis method of sparse nonuniform-amplitude concentric ring arrays for microwave

power transmission," *Progress In Electromagnetics Research C*, Vol. 107, 1–15, 2021.

[15] Li, J., Z. Han, and C. Guo, "Novel subarray partition algorithm for solving the problem of too low beam collection efficiency caused by dividing a few subarrays," *Progress In Electromagnetics Research M*, Vol. 108, 223–235, 2022.

[16] Li, X. and Y.-X. Guo, "Multiobjective optimization design of aperture illuminations for microwave power transmission via multiobjective grey wolf optimizer," *IEEE Transactions on Antennas and Propagation*, Vol. 68, No. 8, 6265–6276, 2020.

[17] Li, X., B. Duan, J. Zhou, L. Song, and Y. Zhang, "Planar array synthesis for optimal microwave power transmission with multiple constraints," *IEEE Antennas and Wireless Propagation Letters*, Vol. 16, 70–73, 2016.

[18] Sun, X., X. Li, K. Liu, and C. Liu, "Study on the transmitting array for ground microwave wireless power transmission system," in *2023 IEEE 11th International Conference on Information, Communication and Networks (ICICN)*, 659–663, 2023.

[19] Guo, H., H. Hao, P. Song, L. Zhang, and X. Zhang, "Synthesis of planar array antenna for wireless power transmission," *Progress In Electromagnetics Research C*, Vol. 121, 163–178, 2022.

[20] Aroniadi, C. and G. N. Beligiannis, "Applying particle swarm optimization variations to solve the transportation problem effectively," *Algorithms*, Vol. 16, No. 8, 372, 2023.

[21] Li, J. and Z. Han, "Synthesis of sparse square arrays with high beam collection efficiency under minimum element spacing constraints," *Microwave and Optical Technology Letters*, Vol. 65, No. 1, 240–246, 2023.

[22] Poli, R., J. Kennedy, and T. Blackwell, "Particle swarm optimization: An overview," *Swarm Intelligence*, Vol. 1, 33–57, 2007.

[23] Miao, A.-M., X.-L. Shi, J.-H. Zhang, E.-Y. Wang, and S.-Q. Peng, "A modified particle swarm optimizer with dynamical inertia weight," in *Fuzzy Information and Engineering*, Vol. 2, 767–776, 2009.

[24] Clerc, M. and J. Kennedy, "The particle swarm-explosion, stability, and convergence in a multidimensional complex space," *IEEE Transactions on Evolutionary Computation*, Vol. 6, No. 1, 58–73, 2002.